Magnetohydrodynamics, Vol. 32, No. 1, 1996

DESIGN OF A LIQUID SODIUM MHD DYNAMO EXPERIMENT

A. Gailitis

The development of an experiment is presented, wherein a liquid sodium flow should generate a magnetic field similarly to the way the convection of the Earth's molten core generates the geomagnetic field.

Introduction. Previously, we had attempted to achieve a magnetic field generation in an electrically more or less homogeneous medium by pumping liquid sodium with an extraneous pump through the experimental model [1]. Inside the model, the stationary baffles imparted to the flow a spiralling characteristic. We were not successful in achieving the calculated flow rate, since an unexpectedly appearing mechanical vibration damaged the welds and the experiment had to be discontinued until the advent of a self-exciting magnetic field.

At the present time, a new experimental model of a different design (Fig. 1) is being fabricated. Instead of an external pump, two electric motors 1 (each rated at 55 kW) turn the turbine 2 inside a cylindrical vessel containing the liquid sodium 3. The lower half of the vertical vessel is situated in the basement of the sodium laboratory. The vessel is divided by thin-walled partitions into three co-axial cylindrical channels A, B, and C. The turbine draws in sodium from channel B and directs it down through the channel A. Having reached the bottom, the flow is turned around and is raised again to the turbine through the channel B. Thus, in the channels A and B a closed flow is maintained. In the channel C, sodium remains stationary, providing closure of the electric currents.

The employed turbine has somewhat lower velocity and steeper blades than the turbines of standard water pumps. Because of that, in channel A, the flow is imparted a significant rotation which is required for the magnetic field generation. Due to inertia, the rotation is preserved down to the lower end of the channel A. After the turn, guide vanes are installed to stop the rotation. In channel B the returning flow is purely axial.

According to the calculations presented below, the model should generate an alternating (rotating) magnetic field when the sodium flow rate is of the order of 0.6 m^3/s.

The Generation Conditions. The calculations are based on a mathematical model, in which the actual flow is replaced by three conductors with length L and with radii $R_A < R_B < R_C$ moving as solid bodies (Fig. 2):

A) A central vortical flow at an axial velocity v_z and rotation ω. The electromagnetic properties of the model are characterized by the dimensionless parameter $Rm = \mu_0 \sigma v_{max} R_A$, $v_{max} = (v_z^2 + \omega^2 R_A^2)^{1/2}$;

B) a uniform return flow without any rotation, returning the entire central stream flow;

C) a stationary conductor.

The thickness of the partitions separating the conductors A from B and B from C is assumed to be zero however their transverse electrical resistances r_{AB} and r_{BC} are included in the boundary conditions and are measured in "equivalent thicknesses of the basic conductor, having equal electrical resistance."

Due to symmetry, the particular solutions of the induction equation exponentially depend on t, z, and φ:

$$B_r \pm iB_\varphi = B_\pm(r)\exp(pt+ikz+i\varphi). \tag{1}$$

In each of the three conductors, as in the external insulator, the radial field dependence is expressed by the Bessel functions [2, 3]:

$$B_\pm(r) = aI_{1\pm1}(cr)+bK_{1\pm1}(cr), \tag{2}$$

Institute of Physics, Latvian Academy of Science, Salaspils-1, LV, Latvia. Translated from Magnitnaya Gidrodinamika, Vol. 32, No. 1, pp. 63-67, January-March, 1996. Original article submitted November 16, 1994.

 0024-998X/96/3201-0058$15.00

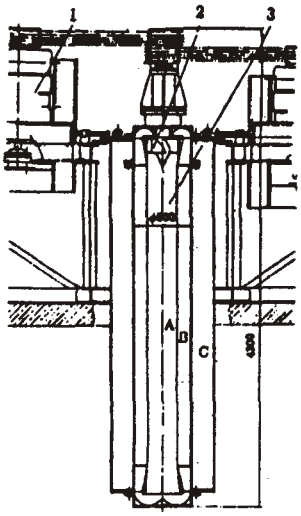

Fig. 1. Schematic of the experiment.
Explanations are provided in the text.

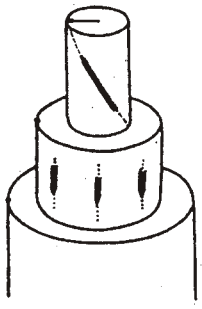

Fig. 2. The mathematical model.

where c is the complex coefficient which is dependent on p, k and on the motion of the given conductor. The consistency of all boundary conditions with a disappearing field at an infinite radius results in a characteristic equation of the type

$$F(\mathrm{Rm}, k_r+ik_i, p_r+ip_i, \text{ geometry}) = 0 \tag{3}$$

F(...) being a cumbersome expression containing Bessel functions of a complex argument,

Equation (3) is solved by numerical iteration. Since the equation is complex, its solution signifies an equation of two actual variables, namely k_r and p_i, as functions of all other arguments Rm, k_i, p_r and of the model geometry.

The analysis of the generation condition is based on Fig. 3, where the dependence of k_r on Rm for $p_r = +0$ is shown for several k_i values. No separate figure is presented for the p_i frequency; however, some information relating to the frequency has been included in Fig. 3. Dotted lines indicate those curve portions where the real part of the complex group velocity $v_{gr} = idp/dk$ is negative. For some Rm, two k_r values are indicated by check marks (the upper lies on the continuous curve, while the lower lies on the dashed curve), which have identical k_i and p_i values.

Stability of the Magnetic Perturbations. From the mathematical viewpoint, the problem of magnetic field generation is a problem concerning the stability of the zero solution of (1). In this case, it is necessary to take into account the magnetic perturbations of two types — the original, which exist at the initial time instant, and those continuously acting from the unsteady magnetic environment. The fate of each perturbation depends on its position in Fig. 3. It is necessary to speak of three critical Rm values, identified in Fig. 3 by one, two, or three asterisks.

$\mathrm{Rm}^* = 15.35$ refers to the extreme-left neutral point of the curve $k_i = 0$, $p_r = +0$. At $\mathrm{Rm} < \mathrm{Rm}^*$, all perturbations attenuate and the zero field represents a stable state for a model of any length. $\mathrm{Rm}^{***} = 18.99$ is a threshold of the actual self-excitation in a model bounded by length $L = 25R_A$ (more details below). $\mathrm{Rm}^{**} = 16.57$ is the self-excitation threshold of an infinitely long model $L = \infty$ and corresponds to the extreme-left point of the involute of the family of curves $k_i = \text{const}$. At

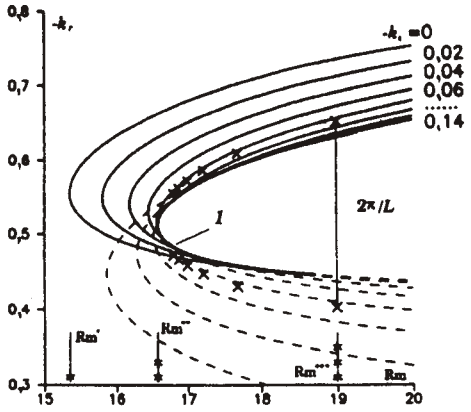

Fig. 3. Numerical solution of Eq. (3): $R_A = 1$, $R_B = 1.77$, $R_C = 3.6$; $\omega = v_z$; $r_{AB} = r_{BC} = 0.08$, × — $L/R_A = 25$, 35, 45, 55, 65, 75. $Rm^* = 15.35$ — onset of the convective instability; $Rm^{**} = 16.57$ — start of absolute instability, i.e., self-excitation for L = 8; $Rm^{***} = 18.99$ — onset of self-excitation for L = 25. 1) involute; continuous line) $Re \mid v_{gr} \mid = Im \mid dp/dk \mid > 0$; dashed line) $Re \mid v_{gr} \mid = Im \mid dp/dk \mid < 0$.

that point, the complex group velocity $v_{gr} = idp/dk$ reduces to zero. Thus, this point is also a Landau saddle point of the function p(k) and the branching point of the inverse function k(p).

At Rm between Rm^* and Rm^{***} all the original perturbations with k_r, falling within the neutral curve, increase with time. However, due to the nonzero group velocity, the perturbation maximum shifts along z and ceases to increase at the instant when the perturbation abandons the model. As a result, what is obtained is not generation but an ultimate amplification. The same also applies to the perturbations from the magnetic surroundings if their frequency is such that $k_i < 0$ and $Re(v_{gr}) > 0$. Along the model length they attain the final amplification $\exp(-k_i L)$.

In other problems (boundary layers and the like), the situation between Rm^* and Rm^{**}, where there is amplification but no feedback, is called convective instability. At significant amplification, the convective instability differs little from the absolute instability ($Rm > Rm^{**}$), where a feedback does exist. Our situation differs from the standard one only by the model length which is insufficient for a significant amplification. In order to observe a generation, it is necessary to have a time-increasing solution which satisfies the zero boundary condition at both model ends.

Below Rm^{**} there exists only one solution (1) but it does not satisfy two conditions. Above Rm^{**} one can find two solutions which for the same Rm, p, and k_i have different $k_r = k_1, k_2$. The sum of the two has zeros at distances $L = 2\pi / \mid k_1 - k_2 \mid$. With an asymptotic ($L >> R_A$) accuracy, L can be taken as the length of a model, where such a solution can be produced.

Optimization. Figure 3 corresponds to the dimensions of the model adopted for realization. These values were selected as the result of some optimization by comparing evaluated Rm^{***} for the various configurations.

Optimization of the dimensions. The flow in the model is achieved in a far-off turbulent region, where the square law of the hydraulic resistance is valid and, in comparison of geometrically similar models, the condition

$$Rm = \mu_0 \sigma v_{max} R_A = \text{const} \tag{4}$$

is equivalent to the condition

$$\text{power} \times \text{dimension} = \text{const.} \tag{5}$$

TABLE 1. Variation of the Critical Rm in Some Model Modifications, $\delta W/100 = (Rm/Rm^{***})^3 - 1$

δRm	δW,%*	Modification	δRm	δW%*	Modification
-1,18	-17	$r_{AB} = 0$	+0,37	+6,0	$(R_A : R_B : R_C)/L = 1{,}65 : 3 : 25$
-0,30	-4,7	$r_{BC} = 0$	-2,42		$L = \infty$

*Percent saving (—), or over-expenditure (+) of the hydraulic power.

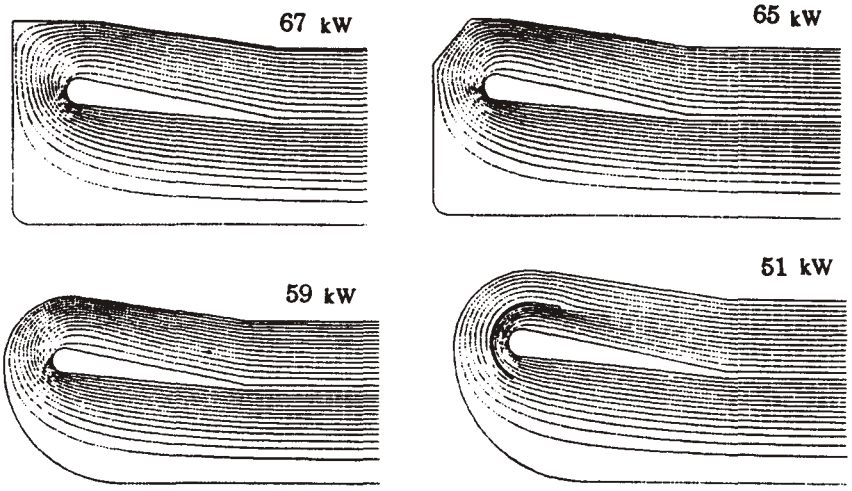

Fig. 4. Flow at the lower turn and the total hydraulic losses for four fairing types.

If all the flow rates related to the experimental arrangement are provisionally divided into flow rates which are proportional to the model volume and those which are proportional to the hydraulic power expended in moving the sodium, then, theoretically, the optimum model size will be the one for which

$$\text{Flow rates} = \text{flow rates [power]}\ (25\%) + \text{flow rates [volume]}\ (75\%). \tag{6}$$

Shape optimization. From the critical Rm calculated in accordance with the mathematical model, the mass minimum and the quadratic resistance law conditions can be derived for the optimum ratio of the active dimension of R_A and the more passive R_C and L:

$$\partial(\ln Rm)/\partial(\ln(R_C/R_A)) = -2/3 \Rightarrow R_C/R_A = 3{,}2;$$

$$\partial(\ln Rm)/\partial(\ln(L/R_A)) = -1/9 \Rightarrow L/R_A = 35.$$

Since the mathematical model does not take into account a certain attenuation of the rotation, L/R_A was lowered to 25, while for technical reasons, R_C/R_A was increased to 3.6.

From the Rm^{***} minimum the following values were selected: $R_B/R_A = 1.77$ = and $\omega R_A/v_z = 1$.

The thicknesses of the separating partitions were chosen based on technical considerations to be 1.5 mm, which in dimensionless electrical resistances signifies that $r_{AB} = r_{BC} = 0.08R_A$. The level of influence of r_{AB}, r_{BC}, R_C, and L is evident from Table 1, where deviations of the critical Rm from the above-mentioned Rm^{***} value and the percent change in the consumed power $\delta W/100 = (Rm/Rm^{***})^3 - 1$, as one of the quantities r_{AB}, r_{BC}, R_C, and L is changed, are presented.

The Hydraulic Calculation. To reach $Rm^{***} = 18.99$ with $R_A = 125$ mm, a flow rate of 0.6 m^3/s is required. To estimate the consumed power, a hydraulic flow loop calculation was performed using the FLUENT program. It was found that the power essentially depends on the design of the lower flow return. Figure 4 shows the flow pattern and the total hydraulic losses over the entire loop for four fairing types without any corrections for the finite turbine efficiency. A notable reduction in the losses is achieved by placing guide vanes in the turns. However, the gain is questionable, since small inaccuracies in their installation lead to a significant rise in the hydraulic resistance.

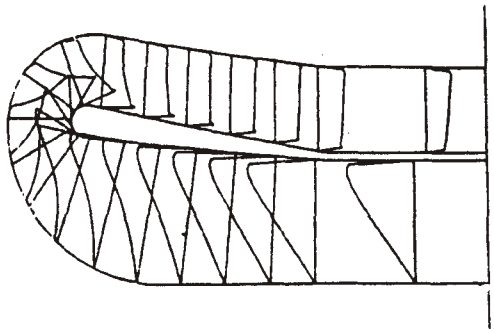

Fig. 5. Azimuthal velocity profiles.

Profiles of the azimuthal velocity before the installation of a straightening cascade behind the turn are presented in Fig. 5. The profile indicates that more than 80 % of the initial rotation is conserved to the end of the straight channel A.

The author is pleased to express his gratitude to the International Science Foundation (Copoc) for financial support under Grants LFD000 and LJD100, without which the formulation of the experiment would have been impossible.

REFERENCES

1. A. K. Gailitis B. G. Karasev, I. R. Kirillov, O. A. Lielausis, S. M. Luzhanskii, and A. P. Ogorodnikov, "An experiment with a liquid metal model of an MHD dynamo," Magn. Gidrodin., No. 4, 3-7 (1987).
2. Yu. B. Ponomarenko, "Theory of the hydromagnetic dynamo," Prikl. Mekh. Tekh. Fiz., No. 6, 47-51 (1973).
3. A. Gailitis and Ya. Feiberg, "Theory of a vortical MHD dynamo," Magn. Gidrodin., No. 2, 3-6 (1976).